Design Principles for Heteroatom-Doped Nanocarbon to Achieve Strong Anchoring of Polysulfides for Lithium–Sulfur Batteries

Ting-Zheng Hou, Xiang Chen, Hong-Jie Peng, Jia-Qi Huang, Bo-Quan Li, Qiang Zhang, and Bo Li**

Lithium–sulfur (Li–S) batteries have been intensively concerned to fulfill the urgent demands of high capacity energy storage. One of the major unsolved issues is the complex diffusion of lithium polysulfide intermediates, which in combination with the subsequent paradox reactions is known as the shuttle effect. Nanocarbon with homogeneous nonpolar surface served as scaffolding materials in sulfur cathode basically cannot afford a sufficient binding and confining effect to maintain lithium polysulfides within the cathode. Herein, a systematical density functional theory calculation of various heteroatoms-doped nanocarbon materials is conducted to elaborate the mechanism and guide the future screening and rational design of Li–S cathode for better performance. It is proved that the chemical modification using N or O dopant significantly enhances the interaction between the carbon hosts and the polysulfide guests via dipole–dipole electrostatic interaction and thereby effectively prevents shuttle of polysulfides, allowing high capacity and high coulombic efficiency. By contrast, the introduction of B, F, S, P, and Cl monodopants into carbon matrix is unsatisfactory. To achieve the strong-couple effect toward Li_2S_x, the principles for rational design of doped carbon scaffolds in Li–S batteries to achieve a strong electrostatic dipole–dipole interaction are proposed. An implicit volcano plot is obtained to describe the dependence of binding energies on electronegativity of dopants. Moreover, the codoping strategy is predicted to achieve even stronger interfacial interaction to trap lithium polysulfides.

T.-Z. Hou, X. Chen, H.-J. Peng, Prof. J.-Q. Huang, Prof. B.-Q. Li, Prof. Q. Zhang
Beijing Key Laboratory of Green Chemical Reaction Engineering and Technology
Department of Chemical Engineering
Tsinghua University
Beijing 100084, China
E-mail: zhang-qiang@mails.tsinghua.edu.cn
Prof. B. Li
Shenyang National Laboratory for Materials Science
Institute of Metal Research
Chinese Academy of Sciences
72 Wenhua Road, Shenyang 110016, P. R. China
E-mail: boli@imr.ac.cn

DOI: 10.1002/smll.201600809

1. Introduction

Given the high theoretical capacity 1672 mAh g^{-1} of sulfur cathode, lithium–sulfur (Li–S) batteries have been intensively concerned to fulfill the urgent demands of high capacity energy storage.[1] Comparing with routine lithium-ion batteries (LIBs), Li–S batteries exhibit advantages of high theoretical energy density of 2600 Wh kg^{-1} (five to seven times higher than that of LIBs), abundant sulfur resources, low cost, high biocompatibility, and extended operating temperature window. While there are notorious issues stemming from low electrical conductivity and volume change of sulfur during cycling, the implementing of sulfur and carbon materials (such as porous carbon,[2] carbon spheres,[3] carbon

nanotubes (CNTs),[4] graphene,[5–7] graphene oxides,[8,9] and their hybrids[10,11]) in sulfur composite cathodes can well ameliorate these issues to a large extent.

However, quite a few obstacles are still hindering the practical applications of Li–S batteries. One of the major issues is the complex diffusion of lithium polysulfide intermediates, which in combination with the subsequent paradox reactions is known as the shuttle effect. Nanocarbon with homogeneous nonpolar surface served as scaffolding materials in sulfur cathode basically cannot afford a sufficient binding and confining effect to maintain lithium polysulfides within the cathode. As a result, high-order lithium polysulfides diffuse through the organic electrolytes, react with the lithium metal anode, and degrade to low-order lithium polysulfides, lowering the available capacity and coulombic efficiency simultaneously. Moreover, the poor electrochemical contact originated from the weak coupling between active polysulfides and conducting scaffolds afflicts the rate performance and exacerbates serious electrode polarization, impeding the rapid and steady cycling of Li–S cells.

Enormous efforts concerning cathode, electrolyte, and separator were explored to alleviate the shuttle effect in systematic management. Solid electrolytes,[12] functional lithium salt additives,[13] and "solvent-in-salt" strategy[14] were found to be able to suppress the shuttle of polysulfides by restricting their solubility in the electrolyte or reactivity toward metallic lithium. Ion-selective separators can also inhibit the polysulfide diffusion by electrostatic/physical repulsion.[15] Nevertheless, the excessive obstruction created by these strategies may impede the ion migration and thereby results in poor reaction kinetics. Moreover, these approaches are still incapable of manipulating effective dynamical electrical contact in the composite cathode during the electrochemical reactions with concomitant complex phase transfer.

Recently, heteroatom doping[3,5,6,11,16–21] and polar compound additives[22–24] are two promising routes in ascendant for the adsorption and immobilization of polysulfide intermediates. Several important materials designed with strong anchoring sites like nitrogen-doped carbon,[3,5,11,17–19] oxygen-functionalized carbon,[8,25] tin-doped indium oxide,[26] transition metal carbides[22] /oxides[23,26] were reported to trap lithium polysulfides via chemical binding. The strong anchoring effect furnished by these concepts not only stabilizes polysulfides within the cathode, but also facilitates the electrochemical contact of polysulfides/scaffold interface.

Although the chemisorption of lithium polysulfides in various porous scaffolds has been achieved worldwide, the origin of the strong anchoring effect is still unclear yet, largely ascribing to the scarceness of a systematic understanding at molecular level where the fundamental descriptors in terms of energetics and kinetics should be determined to preciously depict the interactions at a heterogeneous surface. Theoretical studies were conducted to reveal the chemical nature of interactions between lithium polysulfides and scaffolding materials.[27] Typically interactions in the above-mentioned setups were analyzed in perspectives of binding energy, bond length, charge transfer, charge distribution, and density of state via first principle calculations. However, the analysis would rather be called qualitative unless they described the origin of strong anchoring effect unambitiously. Therefore, a parallel comparison based on analogous theoretical models is still in the absence. Further improvement of the scaffolding materials for sulfur cathode could be achieved by rational materials design only if new insights into the molecular origin of strong chemical binding, the optimized strength of chemisorption, and the method to adapt the binding mechanism were gained from adequate theoretical prediction. Very recently, a systematical investigation on various 2D layered materials (oxides, sulfides, chlorides) was well conducted to describe their detailed interaction with lithium polysulfides.[28] The bond strength between the Li_2S_x species and the substrate was found to be determined by the amount of charge transfer from sulfur atoms in the cluster to the anchoring materials. Similarly, the chemical modification of carbon-based cathodes via heteroatom doping was also widely reported to afford such strong binding interactions with lithium polysulfides,[3,5,11,17–19,21,29] whereas the mechanism was far from full recognition. A systematic consideration of doped nanocarbon materials is in extreme need to guide the rational design of Li–S cathode for better performance.

In this contribution, a series of heteroatom-doped graphene nanoribbons (GNR) was modeled and their binding behaviors toward both polar lithium polysulfide and nonpolar elemental sulfur were evaluated. The first-principle calculation was conducted to systematically describe the complex interactions in terms of different doping atoms. By meticulously analyzing the configuration, binding energy, bond length, charge transfer, and deformation charge density, how the doping atoms including B, N, O, F, P, S, and Cl affect the adsorption of sulfur and Li_2S_x species was explored. The local polarization of binding sites within the carbon lattice was correlated to the subsequent dipole–dipole interactions, both of which were considered to play critical role in the system. A set of principle rules and a volcano plot correlating the electronegativity of doping atoms to the adsorption energies were proposed to guide the future screening and design of scaffolding materials with chemical dopants. In addition, the influence of the electrolyte was also discussed. We proved that proper chemical doping of N/O or even codoping was more favorable to facilitate a better anchoring effect.

2. Results and Discussion

Graphene and CNTs used as sulfur scaffolds are usually abundant in edges and boundaries where heteroatoms (e.g., N, O, B, etc.) are easily incorporated into the carbon lattice and enriched during the synthesis. Due to their structural resemblance to simulate the copious boundary and edge regions of CNTs and graphene, GNRs, which consist of nanometer-sized stripes of graphene sheets, are suitable materials platform for precious and self-consistent theoretical prediction of aforementioned various heteroatom-doped carbon frameworks.[30] Consequently, we constructed a series of periodical GNR models (Figures S1–S4, Supporting Information) for the doped nanocarbon that varies from different chemical environments of each heteroatom experimentally

validated by the high-resolution spectra of X-ray photoelectron spectroscopy results.[31] **Figure 1**a gives a schematic illustration of X-doped nanocarbon materials (X = B, N, O, F, P, S, Cl), where a considerable amount of dopants including pyridinic nitrogen (pN), pyrrolic nitrogen (rN), graphitic nitrogen (gN), ketone group (kO), carboxylic group (aO), epoxy group (eO), cyclic oxygen (cO), hydroxyl group (hO), graphitic boron (gB), B-2C-O type boron (oB), fluorine (F), phosphorus (P), chlorine (Cl), sulfur (S), and sulfonyl group (oS) are incorporated into the carbon lattice and marked as different colors.

Each kind of dopant was modeled, respectively, into a GNR cell that contains 30 hexagonal sp^2-carbon rings saturated with terminal hydrogen, corresponding to an atomic doping concentration of 1.4–2.8 at%. The seven considered heteroatoms render 15 different doping configurations of GNRs with very different affinities toward polysulfides. Li_2S, Li_2S_4, Li_2S_8 clusters, and S_8 molecule are allowed to interact with the 15 kinds of doped GNRs.

The binding energy, configuration, bond length, differential charge density, and solvation effect were explicitly examined on the basis of density functional theory (DFT) calculations. The simulated binding energies (E_b) are summarized in Figure 1b and Tables S1 and S2 (Supporting Information). The adsorption of polar species (Li_2S, Li_2S_4, Li_2S_8) is quite sensitive to dopant elements according to the largely varied E_b. GNRs with N and O dopants, especially pN-GNR, aO-GNR, and kO-GNR, exhibit relatively larger binding energies of –2.53 to –2.56 eV than undoped GNR of –1.93 to –1.95 eV toward Li_2S_4 and Li_2S_8, the representative low-order and high-order polysulfides, raising the binding energy by about 0.6 eV. The result proves that precious functionalization with optimized groups of carbon materials is beneficial for anchoring these soluble intermediates. During cycling of Li–S batteries, the N/O-doped carbon can trap soluble intermediates and retard the shuttle of polysulfides, which is consistent with previous results collected by both experimental testing and theoretical calculation.[3,5,8,11,17–19,25,27] For instance, N-doped graphene paper electrode[19] exhibited high specific capacity of ≈1000 mAh g^{-1} after 100 cycles and excellent coulombic efficiency of 98% for catholyte-type Li–S cell. N-doped graphene[18] also enabled sulfur composite cathode to deliver high specific discharge capacities of 1167, 1058, 971, 802, and 606 mAh g^{-1} at current rate of 0.2, 0.5, 1.0, 2.0, and 5.0 C, respectively. A much extended cycle life over 2000 cycles and an extremely low capacity-decay rate of 0.028% per cycle can thus be achieved. Moreover, the strong interaction between graphene oxide and polysulfides also achieved Li–S cells with a high reversible capacity of 950–1400 mAh g^{-1}, and stable

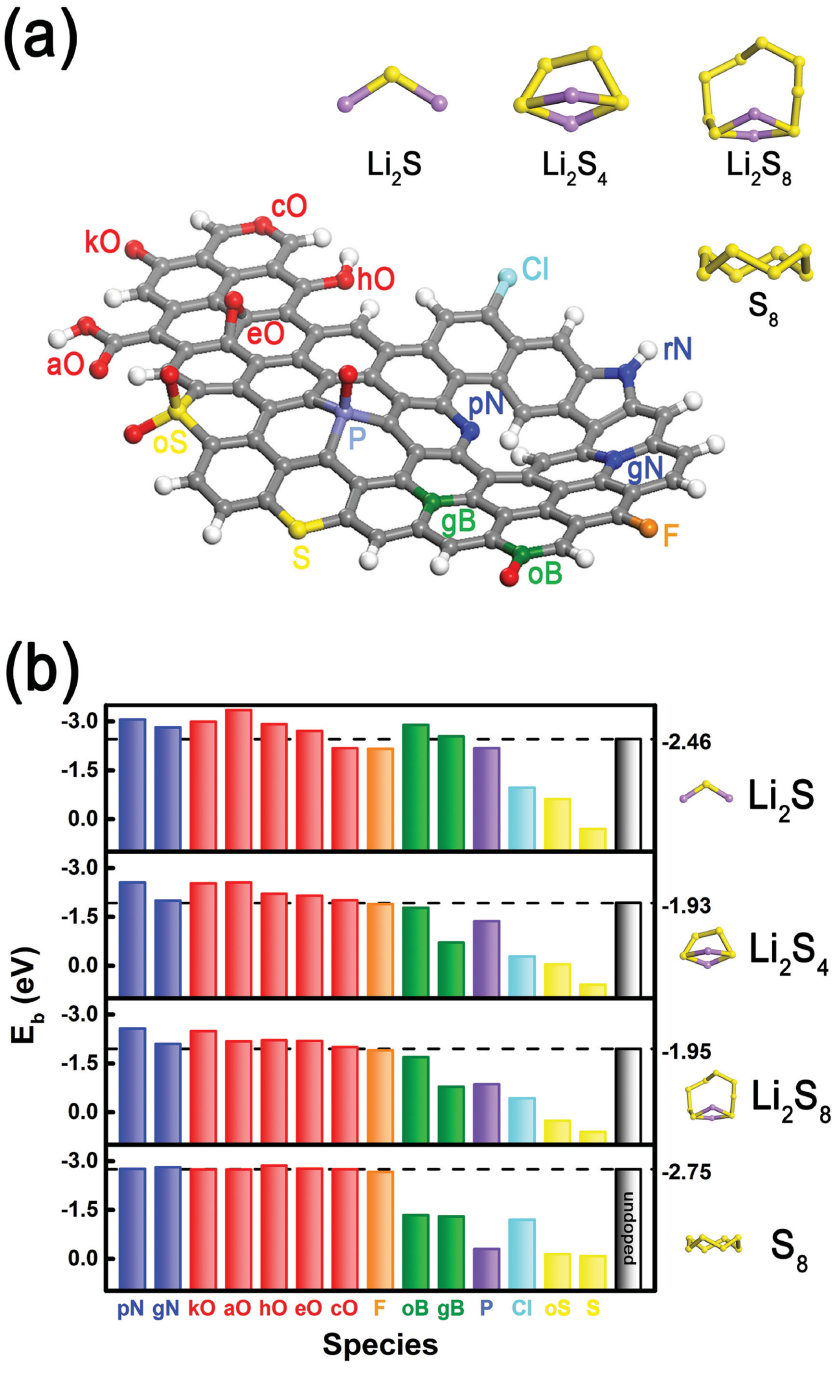

Figure 1. a) The schematic diagram of X-doped nanocarbon materials (X = N, O, F, B, P, S, Cl) and PBE level optimized structure of Li_2S, Li_2S_4, Li_2S_8, S_8 molecules, which are key intermediates in the charge/discharge process of Li–S battery. b) The binding energy E_b (eV) of Li_2S, Li_2S_4, Li_2S_8, and S_8 interacting with X-doped GNRs with zigzag edge, and the binding energies of Li_2S, Li_2S_4, Li_2S_8, and S_8 interacting with pristine (undoped) GNR are shown as grey bars and dashed lines for reference. The carbon, hydrogen, nitrogen, oxygen, fluorine, boron, phosphorus, chlorine, lithium, and sulfur elements are represented by grey, white, blue, red, orange, green, lavender, cyan, purple, and yellow, respectively.

cycling for more than 50 deep cycles at 0.1 C. Thus, benefiting from N/O-doping and correspondingly enhanced interfacial interaction, the practical performance of carbon cathode hosts for Li–S battery was significantly better than that of undoped graphene. The theoretical prediction and the experimental result corroborated well with each other to a very large extent.

As for the adsorption of Li_2S molecule, aO-GNR exhibited the highest binding energy among the 15 species. According to the general growth behavior of nanoparticles, a higher binding energy toward precursor monomers is beneficial for the crystallization by lowering the surface tensile against the substrate and enhancing nucleation. The active sulfur-containing compounds thus are expected to be fully participated in the electrochemical deposition process, which manifests as higher capacity according to the Faraday Law and better rechargeability of Li_2S as the result of enhanced attachment. Furthermore, the accelerated nucleation enables faster kinetics and benefits the rate performance of a sulfur cathode. While oB-GNR exhibits a high binding energy of Li_2S, its binding energies toward Li_2S_4 and Li_2S_8 are low due to the geometrical limitation. Consequently, such B dopants are not as efficient as N or O dopants for alleviating the shuttle effect and thereby ought to be a less considered modification for carbon scaffolds.

Similar to B, other investigated elements are unsatisfactory to provide adequate interactions between carbon hosts and Li_2S_x guests. The binding energies of F-doped GNR with Li_2S_x were almost equal to those of undoped GNR, indicating that F monodoping might be a futile effort in the perspective of modified interaction at the cathode interface. The situation is even worse for P, S, and Cl-doped GNR: their binding energies with Li_2S_x are much lower than that of undoped GNR. One may think that S monodoping would benefit strong affinity toward Li_2S_x, inspired by its successful implementation in oxygen reduction reactions through additional spin effect beyond common N doping.[32] However, the result here lies on the opposite side and well explains why a recent effort to exploit the feasibility of S-modified graphene as sulfur scaffolds was complemented with N dopants, as S dopants cannot solitarily afford the efficacy of strengthening the interaction.[6]

According to our theoretical prediction, N, O, F-doped GNRs exhibit similar binding energies for S_8 molecules to the undoped counterpart, illustrating that the binding state of nonpolar S_8 was insensitive to the introduction of these three elements. However, in the cases of B, P, S, and Cl, the binding energies unfortunately decrease, suggesting the negative influence on the strong anchoring behavior. We also observed that eO-GNR tended to interact with S_8 molecule from the opposite direction of the functional group with respect to the carbon plane (Figure S5a, Supporting Information).

To further ascertain the binding state of polysulfide adsorbates over each heterodoped GNR, we scrutinized the bond length between each adsorption pair. Among all the Li_2S_x species, Li_2S_4 is believed to be the key intermediate involved in the Li–S redox.[33] Therefore, we focused on the adsorption geometry of Li_2S_4 as a paradigm to explore the origin of strong-coupling effect of N and O-modified GNRs and the relatively weaker interactions afforded by other dopants. Li_3N and Li_2O crystal models were built as a benchmark of Li—N or Li—O bond length with O or N-doped GNRs.

As shown in **Figure 2**a–i, the Li—N and Li—O distances in the adsorption geometry are similar to the corresponding bond length in crystal, solidifying the so-called strong interactions. However, as for the gB-GNR (Figure 2j), the binding is weak and bond length is large. Other forms like Cl-GNR (Figure 2n) and S-GNR (Figure 2o) where a third-row element binds directly with Li_2S_4 display very long bond distances and are not stable. The radii of dopant atom in such configurations are too large to match with lithium and cannot form a stable chemisorption. Moreover, in the case of oB (Figure 2k) and oS (Figure 2p), the introduction of a Li_2S_4 guest damages the original configuration as there is a major change of C—C—B or C—C—S bond angle.

Due to the higher electronegativity of F atom (3.98), O atom (3.44), N atom (3.07) against Li atom (0.98), the interactions between these atoms and Li are largely analogous to the so-called "Li bond" which can be well explained by the Lewis acid–base theory.[34] The pN-, kO-, F-GNRs with extra pair of electrons are considered as electron-rich donors with filled *p* orbitals that naturally act as a Lewis-base sites to interact with strong Lewis acid of terminal Li atoms in lithium (poly)sulfides. However, the binding energy of F-GNR is poorer than N and O-doped GNRs, hinting at a difference in their chemical state. The different binding states are validated by the population analysis and electron density around the local binding sites. Particularly, the changes of Mulliken charge distribution for pN-, kO-, F-GNRs are illustrated in **Figure 3**a,b,d,e,g,h. F, O, and N all have a higher electronegativity than C (2.55), so these three atoms are all negatively charged and form dipole moments within the conjugated sp^2-carbon lattice. Although F is the most electronegative, the charge at the local binding site is the least due to its different molecular orbitals. All the three kinds of atom form σ-bonds with adjacent carbon, withdrawing electron by inductive effect. However, the filled *p* orbitals of F form a p–π conjugation structure with the carbon plane that feedbacks electron from F to carbon. The combined electron-withdrawing σ and electron-releasing p–π effect reduces the negative charge on F. In contrast, both N and O atom herein can not only withdraw electron from σ interaction, but also participate in the delocalized π system of GNR that additionally contributes to their negative charge. Moreover, after being polarized by the Li_2S_4, O and N withdraw even more electron of 0.06 and 0.12 e from the conjugated system, respectively, while F only accepts 0.03 e. Generally, dopant atoms in both pN-GNR and kO-GNR enjoy more negative charge than F, especially when a Li-GNR interaction is formed. Consequently, both polarity and dipole moment of kO-GNR and pN-GNR are much stronger than F-GNR. A strong dipole–dipole interaction is expected for kO-GNR and pN-GNR to adsorb Li_2S_4, achieving a larger binding energy compared with F-GNR.

Figure 3c,f,i illustrates the deformation charge density corresponding to the Li_2S_4 adsorption site in which the increase and decrease of total electron density with respect to the density of isolated atoms are denoted as blue and red, respectively. For pN-, kO-, and F-GNRs, terminal Li atoms in Li_2S_4 tend to directly bind to the N, O, or F atom. There

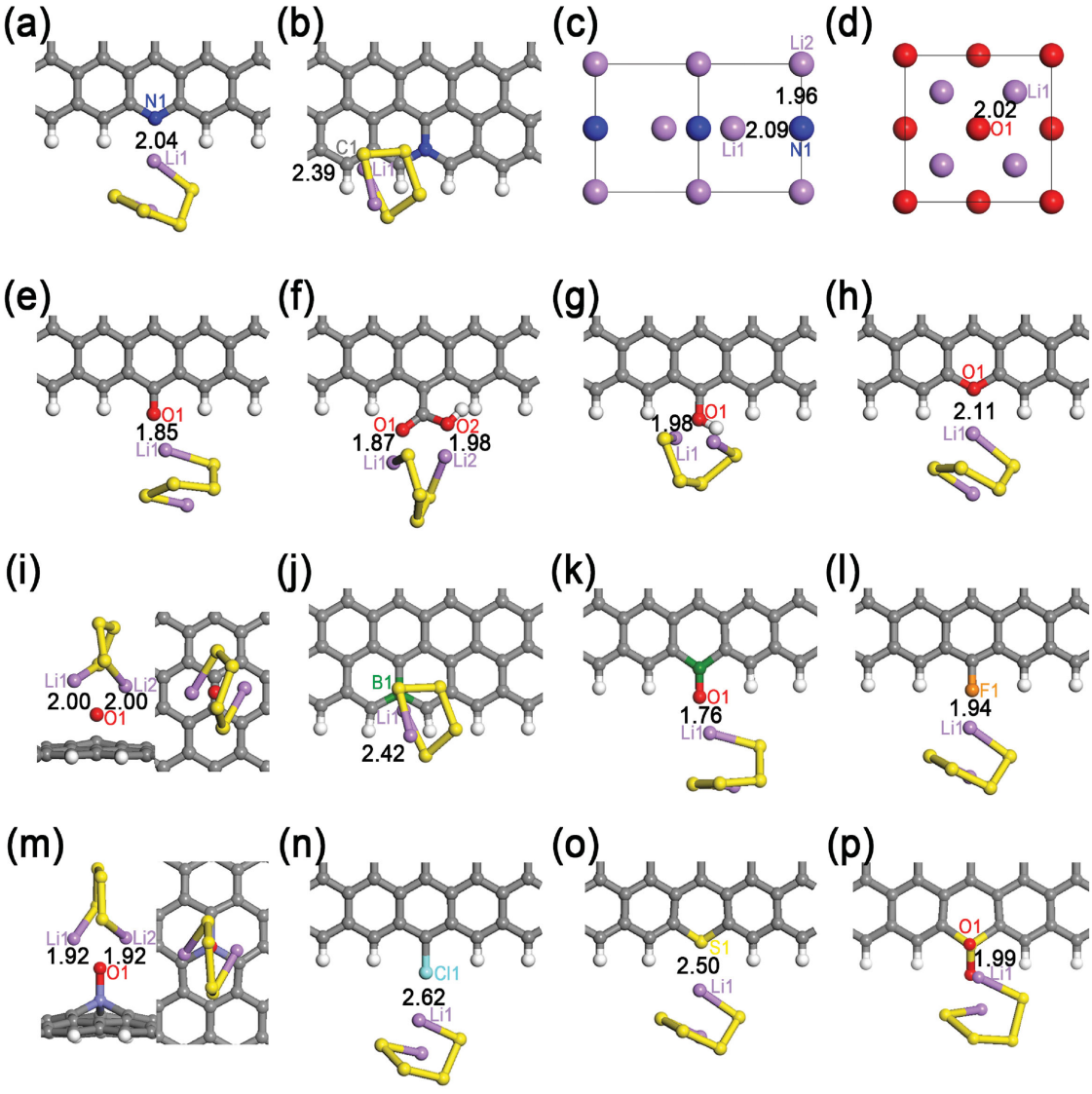

Figure 2. The optimized interaction geometry of Li_2S_4 and a) pN-GNR, b) gN-GNR, c) Li_3N, d) Li_2O, e) kO-GNR, f) aO-GNR, g) hO-GNR, h) cO-GNR, i) eO-GNR, j) gB-GNR, k) oB-GNR, l) F-GNR, m) P-GNR, n) Cl-GNR, o) S-GNR, and p) oS-GNR, relatively. The marked atoms are the nearest atoms between the host and guest, and their distances are as shown.

is distinctive electron concentration manifesting the lone pair electrons of N/O atom that interact with Li atom and afford a strong Li—N/O ionic bond interaction. However, the electron density variation around F is relatively insignificant. Moreover, by examining the Mulliken charge distribution, we found that there is only a minor contribution to charge transfer between the heterodoped carbon basal plane and Li_2S_4, which further indicates the electrostatic nature of Li—N/O interactions. Therefore, the strength of electrostatic dipole–dipole interaction emerges as the pivotal descriptor to determine the interaction between heterodoped GNRs and Li_2S_4. In this perspective, N and O-doped GNRs beat all other forms of monodoped GNRs including F-GNR, though the F atom has the most electronegativity among all nonmetallic elements.

Compared to C atoms in the graphene lattice, gN is also an electron-rich donor and is expected to increase the local charge density at the doping region. However, different from pN, gN provides its *p* electrons to the π-conjugated system and is not able to afford additional lone pair electron entirely for adsorbing Li_2S_4. The electron originated from the N is highly delocalized on the whole plane. Thus, the potential ability for the *p* electron pair to attract Li_2S_4 where a graphitic C atom is substituted by a N atom is weakened especially for larger conjugated system like GNRs than some simplified molecules with less aromatic rings that was modeled by us previously.[35] As a result, the effect of gN-GNR is not as positive as that of pN-GNR and kO-GNR in terms of the relatively weaker binding energy. Similarly, as indicated in Table S2 (Supporting Information), rN-GNR plays an analogous role as pN-GNR.

The B atom in gB-GNR cannot afford a lone pair of electrons since it only has three valence shell electrons, indicating that B is rather an electron acceptor than a donor when incorporated into the carbon lattice. This explains why the gB-GNR only provides a relatively weak binding energy of

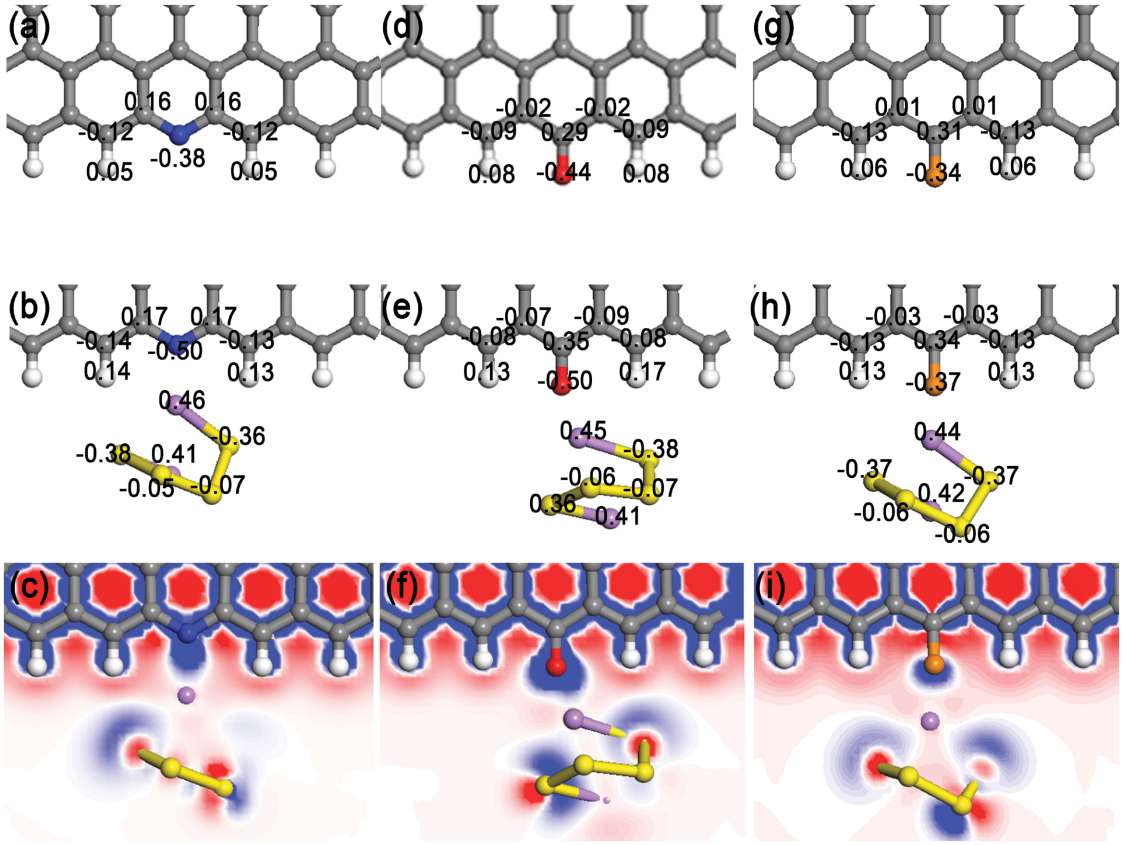

Figure 3. The Mulliken charge distribution before and after adsorption, and the corresponding deformation charge density at Li_2S_4 adsorption site of a–c) pN-GNR, d–f) kO-GNR, and g–i) F-GNR, respectively. The increase/decrease of total electron density with the density of isolated atoms subtracted is denoted as blue/red, respectively.

–0.78 eV. As for Cl- and S-GNRs, they either enjoy a relatively low electronegativity or large bond length although the doping atoms have lone pair electrons, which cannot ensure pure electrostatic interaction.

During geometry optimization process, parasitic reactions occur in the eO-GNR (Figure S5b,c, Supporting Information) and hO-GNR (Figure S5d, Supporting Information). The reactions observed herein reveal that the interactions between GNR and epoxy group or hydroxyl group are quite weak, so carbon materials functionalized with epoxy group or hydroxyl group are not stable enough to withstand the attack of Li_2S_4 or Li_2S during cycling. Therefore, only kO-GNR, aO-GNR, and cO-GNR can serve as stable O-doped nanocarbon materials to stabilize lithium polysulfides. This explains the previous experimental results that O-doped CNT cathode initially enjoy a high initial capacity but decay very rapid.[35]

According to the insights gained from Figures 2 and 3, we can conclude several rules of favoring a strong anchoring effect for doped nanocarbons:

(1) The doping atom should have a lone pair of electrons to serve as a Lewis base to interact with the Lewis acidic lithium polysulfide. Therefore the B monodoping is inappropriate to suppress the shuttle effect.
(2) The electronegativity of the doping atom should be higher than C to allow a permanent dipole moment at the local doping site. Meanwhile, the radius of the doping atom ought to be sufficiently small to pair with Li, thus facilitating an electrostatic dipole–dipole interaction over the Li—doping atom bond with appropriate length. Such intermolecular interaction is in favor of the strong binding strength between Li and high-electronegativity atoms according to the Li bond theory. Thus, only second-row elements are eligible candidates of dopant in the perspective of the electronegativity and the radius.
(3) The doping atom that forms a π bond with the conjugated system is capable of accepting additional charge from the π electrons, thus strengthening the dipole–dipole interaction.
(4) The bond between the doping atom and the carbon matrix should enjoy a high bond stability. Otherwise, the materials would react with Li_2S_4 irreversibly, further undermining the binding toward Li_2S_4.

Based on these considerations, N is better than O as a monodopant to retard the shuttle effect as observed by experiment.[35]

In a practicable Li–S battery, cathode materials work in an organic solvent environment. To examine the influence of electrolytes during charge and discharge process, we tried to compare the binding energies of pN-GNR, kO-GNR, undoped GNR, two 1,3-dioxolane (DOL) molecules,

and two dimethoxyethane (DME) molecules toward Li_2S_4, respectively, and all these calculations were conducted by adopting the continuum conductor-like screening model (COSMO)[36] to describe the solvent environment. The widely used DOL/DME (1:1) electrolytes were chosen as the continuum solvent, and the dielectric constant was obtained from the arithmetical mean of DOL (7.1) and DME (7.2).[37] As shown in **Figure 4**a, the binding energy of undoped GNR is roughly equivalent to that of solvent molecules, indicating that the Li_2S_4 cannot be strongly anchored to the GNR matrix and easily dissolves into the solution phase. However, the binding energies of pN-GNR and kO-GNR exceed the DOL or DME by about 0.6 eV, suggesting that the anchoring effect of pN and kO will surpass the dissolution. Thus, as illustrated in Figure 4a, the strong-coupled interfaces formed by pN-GNR and kO-GNR are fully justified, which can resist the solvation effect, immobilize the Li_2S_x species on the carbon host, and alleviate the shuttle of polysulfides in principle.

Considering the above-discussed rules, an implicit volcano plot (Figure 4b) was obtained by plotting E_b versus the electronegativity of second-row nonmetallic atoms as dopants. This is not just a phenomenological rule, but can be well explained. With the increase of electronegativity (also the proton number and spare electrons), more negative charge is available on the doping atom within the carbon lattice to form a dipole moment that interacts with the Li_2S_x. However, as the atom approaches the closed shell structure (like F), its bonding power weakens, depriving of its capability to withdraw electrons from the conjugated plane and thereby undermining the binding energy as the result of less local polarization. Therefore as depicted, the summit of the plot locates between N and O. As for third-row doping elements, their binding energies toward Li_2S_x are too low to be included in the plot, indicating their poor ability as monodopants for nanocarbon scaffolding materials to alleviate Li_2S_x shuttle in Li–S batteries.

If we go step further from the rules to seek a breakthrough beyond the volcano plot of monodoped GNRs, there is codoped nanocarbon in which two or more dopants adjacent to each other synergistically strengthen the dipole moment and offer even better affinity to Li_2S_x dipoles. Based on this consideration, we built a (N, O) codoped GNR in which N and O atoms influenced the properties of GNR by synergy (Figure S6, Supporting Information). The calculation result exhibits that the binding energy toward Li_2S_4 is –3.18 eV (Figure 4b), which is well in accordance with the prediction that codoping facilitates a stronger anchoring interaction as the result of stronger dipoles. Consequently, in a perspective of strong-couple interaction, codoped carbon is a good candidate for scaffolding materials in Li–S batteries with strong anchoring sites for polysulfides. Thus, a Li–S battery with high specific discharge capacity, long cycle stability, and superb coulombic efficiency could be achieved. Very recently, pioneer works on (S, N) codoped and (B, O) codoped carbon cathode was reported to have excellent electrochemical performance,[6,21] corroborating our calculation and predication to a very large extent. It was reported that the predicted E_b of (B, O) codoped carbon cathode (BC_2O, BCO_2, and B_2O_3 type) are substantially greater than those at the monodoped O and N sites.[21] Significantly improved capacity, rate performance, and cycle stability have been achieved compared to the undoped ones in Li–S batteries. What

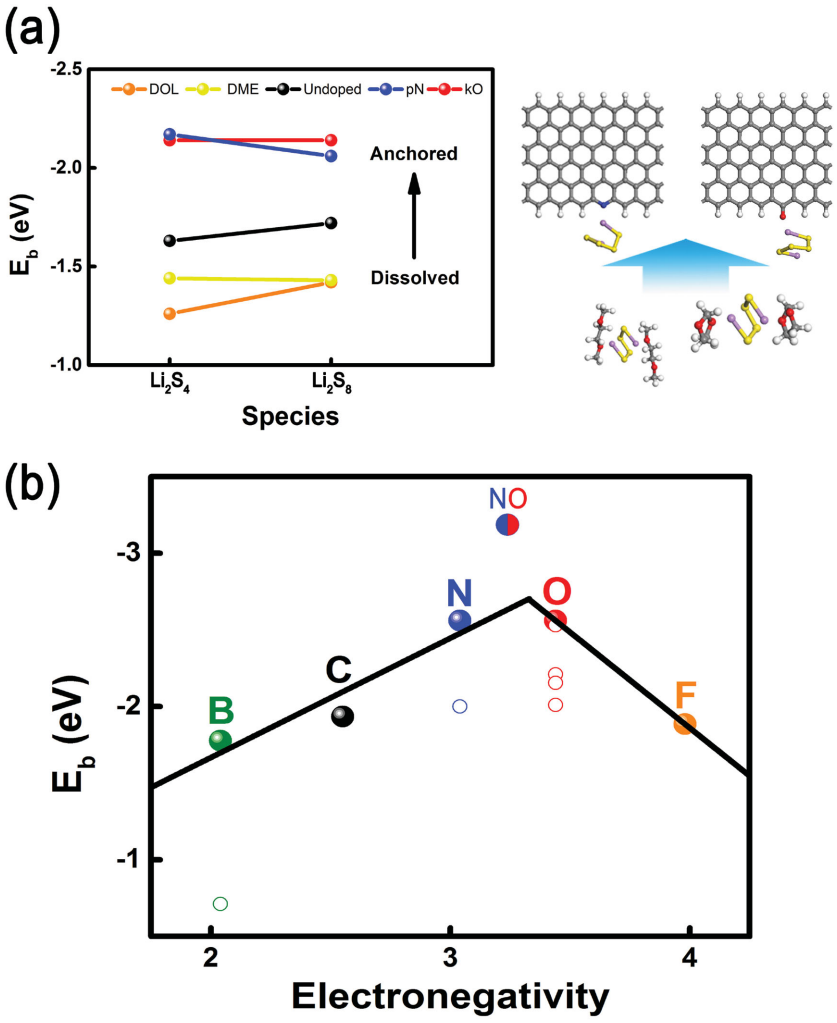

Figure 4. a) The E_b of Li_2S_4/Li_2S_8 interacting with certain doped GNR, undoped GNR, and DOL/DME solvent. The schematic diagram shows how strong-coupled interaction is formed by certain doped GNR that alleviates the interactions between polysulfides and solvents as well as the consequent dissolution. b) The E_b with Li_2S_4 versus electronegativity of dopant elements (carbon for the undoped) of GNRs. The E_b of (N, O) codoped GNR with Li_2S_4 is also shown for comparison. The solid circle indicates the E_b of the chemical form with the highest E_b of certain elements, and the hollow circle indicates the E_b of other chemical forms of certain elements.

is more, DFT results[6] clearly demonstrated that the coexistence of N and S can significantly enhance the binding of lithium polysulfides, when compared with the undoped or single N/S-doping cases. The (N, S) codoped graphene electrode with a high sulfur loading of 4.6 mg cm^{-2} exhibited fast reaction dynamics, reduced polarization, and stabilized cycling performance with only 0.078% capacity decay per cycle up to 500 cycles.

3. Conclusion

In summary, by forming an analogue of "Li bond," the chemical modification using N or O dopant significantly enhances the interaction between the carbon host and the polysulfide guests and thereby effectively prevent shuttle of polysulfides, allowing high capacity and high coulombic efficiency. Both N and O heteroatoms with extra pair of electrons are considered as electron-rich donors that naturally acted as a Lewis-base sites to interact with strong Lewis acid of terminal Li atoms in lithium (poly)sulfides via dipole–dipole electrostatic interaction. In contrast, the introduction of B, F, S, P, and Cl monodopants into carbon matrix is unsatisfactory, which was barely reported experimentally.[20,21] To achieve the strong-couple effect toward Li_2S_x, the principles for rational design of doped carbon scaffolds in Li–S batteries are summarized as: (1) the doping atom has a lone pair electron; (2) the doping atom exhibits a higher electronegativity than carbon and a small radius that matches Li; (3) the doping atom forms a delocalized π bond with the conjugated system; (4) the doping atom forms a stable bond to the carbon plane. With these conditions fulfilled, the carbon host could offer a strong dipole with lone pair election to form a strong electrostatic dipole–dipole interaction with Li_2S_4, verifying the calculation and experiment results that N and O doping are the better choice to relieve the shuttle effect. An implicit volcano plot can be obtained to describe the dependence of binding energies on electronegativity of dopants. Beyond the maximum limit of the plot of monodoped GNRs, the codoping strategy is predicted to achieve even stronger interfacial interaction to trap lithium polysulfide.

4. Experimental Section

The binding energy, configuration, bond length, and differential charge density between heteroatom doped GNR and lithium polysulfide/elemental sulfur were examined on the basis of DFT calculations performed by DMol3 package.[38] All the calculations were carried out using Perdew–Burke–Ernzerhof (PBE) exchange-correlation functions[39] in the framework of general gradient approximation with all atoms fully relaxed. An all-electron double numerical basis set with polarization functions was used in this contribution. The convergence criteria applied for geometry optimizations were 2.0×10^{-5} au, 4.0×10^{-3} au $Å^{-1}$, and 5.0×10^{-3} Å for energy change, maximum force, and maximum displacement, respectively. The threshold for self-consistent-field density convergence was set to 1.0×10^{-5} eV. K point was set to $8 \times 1 \times 1$, which was verified by the convergence test as shown in Figure S7 (Supporting Information). The vacuum layer along the normal direction and the slip direction of the nanoribbon was set to 20 Å, which was examined to be large enough to avoid unexpected interactions between atoms in different super cells.

As described above, substitutional impurities tend to concentrate on the edge. To further testify the predominant substitutional sites of dopants, two sets of structural models of nanoribbon with gN and gB on two different substitutional sites were tested (Figure S8, Supporting Information). The result indicated that both gN and gB energetically preferred to lie on the edge. Therefore, we adopted the model that gN and gB that is near the edge, rather than in the middle. The solvent (DOL/DME) effect was also embraced in this contribution when considering the competition between cathode and solvent to combine Li_2S_4 by taking the COSMO model.

For a quantitatively description of the interactions between the nanoribbons and the S-containing clusters, the binding energy E_b was defined as follows

$$E_b = E_{total} - (E_{GNR} + E_S) \quad (1)$$

E_{total}, E_S, and E_{GNR} represented the total energies of a nanoribbon, an isolated sulfur-containing cluster (Li_2S, Li_2S_4, Li_2S_8 clusters or S_8 molecule), and a certain nanoribbon binding to a S-containing cluster, respectively. The higher absolute value of binding energy corresponded to stronger interaction.

Supporting Information

Supporting Information is available from the Wiley Online Library or from the author.

Acknowledgements

This work was supported by the National Natural Science Foundation of China (21306103 and 21422604), National Basic Research Program of China (2015CB932500), Tsinghua University Initiative Scientific Research Program (2014z22076), and Tsinghua National Laboratory for Information Science and Technology.

[1] a) A. Manthiram, S. H. Chung, C. X. Zu, *Adv. Mater.* **2015**, *27*, 1980; b) M. A. Pope, I. A. Aksay, *Adv. Energy Mater.* **2015**, *5*, 1500124; c) L. Ma, K. E. Hendrickson, S. Y. Wei, L. A. Archer, *Nano Today* **2015**, *10*, 315; d) J.-Q. Huang, Q. Zhang, F. Wei, *Energy Storage Mater.* **2015**, *1*, 127; e) R. Xu, J. Lu, K. Amine, *Adv. Energy Mater.* **2015**, *5*, 1500408; f) J. Liang, Z.-H. Sun, F. Li, H.-M. Cheng, *Energy Storage Mater.* **2016**, *2*, 76.
[2] X. Ji, K. T. Lee, L. F. Nazar, *Nat. Mater.* **2009**, *8*, 500.
[3] G. M. Zhou, Y. B. Zhao, A. Manthiram, *Adv. Energy Mater.* **2015**, *5*, 1402263.
[4] X. B. Cheng, J. Q. Huang, Q. Zhang, H. J. Peng, M. Q. Zhao, F. Wei, *Nano Energy* **2014**, *4*, 65.
[5] Z. Y. Wang, Y. F. Dong, H. J. Li, Z. B. Zhao, H. B. Wu, C. Hao, S. H. Liu, J. S. Qiu, X. W. Lou, *Nat. Commun.* **2014**, *5*, 5002.
[6] G. M. Zhou, E. Paek, G. S. Hwang, A. Manthiram, *Nat. Commun.* **2015**, *6*, 7760.

[7] L. F. Fei, X. G. Li, W. T. Bi, Z. W. Zhuo, W. F. Wei, L. Sun, W. Lu, X. J. Wu, K. Y. Xie, C. Z. Wu, H. L. W. Chan, Y. Wang, *Adv. Mater.* **2015**, *27*, 5936.
[8] L. W. Ji, M. M. Rao, H. M. Zheng, L. Zhang, Y. C. Li, W. H. Duan, J. H. Guo, E. J. Cairns, Y. G. Zhang, *J. Am. Chem. Soc.* **2011**, *133*, 18522.
[9] Z. W. Seh, H. Wang, N. Liu, G. Zheng, W. Li, H. Yao, Y. Cui, *Chem. Sci.* **2014**, *5*, 1396.
[10] a) M. Q. Zhao, X. F. Liu, Q. Zhang, G. L. Tian, J. Q. Huang, W. C. Zhu, F. Wei, *ACS Nano* **2012**, *6*, 10759; b) H. J. Peng, J. Q. Huang, M. Q. Zhao, Q. Zhang, X. B. Cheng, X. Y. Liu, W. Z. Qian, F. Wei, *Adv. Funct. Mater.* **2014**, *24*, 2772.
[11] J. X. Song, M. L. Gordin, T. Xu, S. R. Chen, Z. X. Yu, H. Sohn, J. Lu, Y. Ren, Y. H. Duan, D. H. Wang, *Angew. Chem. Int. Ed.* **2015**, *54*, 4325.
[12] Z. Lin, C. D. Liang, *J. Mater. Chem. A* **2015**, *3*, 936.
[13] D. Aurbach, E. Pollak, R. Elazari, G. Salitra, C. S. Kelley, J. Affinito, *J. Electrochem. Soc.* **2009**, *156*, A694.
[14] L. Suo, Y. S. Hu, H. Li, M. Armand, L. Chen, *Nat. Commun.* **2013**, *4*, 1481.
[15] a) L. Zhou, X. Lin, T. Huang, A. Yu, *J. Mater. Chem. A* **2014**, *2*, 5117; b) J. Q. Huang, T. Z. Zhuang, Q. Zhang, H. J. Peng, C. M. Chen, F. Wei, *ACS Nano* **2015**, *9*, 3002.
[16] a) H. J. Peng, Q. Zhang, *Angew. Chem. Int. Ed.* **2015**, *54*, 11018; b) Q. Pang, J. T. Tang, H. Huang, X. Liang, C. Hart, K. C. Tam, L. F. Nazar, *Adv. Mater.* **2015**, *27*, 6021.
[17] a) W. D. Zhou, C. M. Wang, Q. L. Zhang, H. D. Abruna, Y. He, J. W. Wang, S. X. Mao, X. C. Xiao, *Adv. Energy Mater.* **2015**, *5*, 1401752; b) J. X. Song, T. Xu, M. L. Gordin, P. Y. Zhu, D. P. Lv, Y. B. Jiang, Y. S. Chen, Y. H. Duan, D. H. Wang, *Adv. Funct. Mater.* **2014**, *24*, 1243; c) C. Tang, Q. Zhang, M. Q. Zhao, J. Q. Huang, X. B. Cheng, G. L. Tian, H. J. Peng, F. Wei, *Adv. Mater.* **2014**, *26*, 6100; d) X. X. Gu, C. J. Tong, C. Lai, J. X. Qiu, X. X. Huang, W. L. Yang, B. Wen, L. M. Liu, Y. L. Hou, S. Q. Zhang, *J. Mater. Chem. A* **2015**, *3*, 16670; e) S. Xiao, S. Liu, J. Zhang, Y. Wang, *J. Power Sources* **2015**, *293*, 119.
[18] Y. C. Qiu, W. F. Li, W. Zhao, G. Z. Li, Y. Hou, M. N. Liu, L. S. Zhou, F. M. Ye, H. F. Li, Z. H. Wei, S. H. Yang, W. H. Duan, Y. F. Ye, J. H. Guo, Y. G. Zhang, *Nano Lett.* **2014**, *14*, 4821.
[19] K. Han, J. Shen, S. Hao, H. Ye, C. Wolverton, M. C. Kung, H. H. Kung, *ChemSusChem* **2014**, *7*, 2545.
[20] a) C. P. Yang, Y. X. Yin, H. Ye, K. C. Jiang, J. Zhang, Y. G. Guo, *ACS Appl. Mater. Interfaces* **2014**, *6*, 8789; b) Y. Xie, Z. Meng, T. Cai, W. Q. Han, *ACS Appl. Mater. Interfaces* **2015**, *7*, 25202; c) A. Vizintin, M. Lozinšek, R. K. Chellappan, D. Foix, A. Krajnc, G. Mali, G. Drazic, B. Genorio, R. Dedryvère, R. Dominko, *Chem. Mater.* **2015**, *27*, 7070.
[21] G. Zhou, E. Paek, G. S. Hwang, A. Manthiram, *Adv. Energy Mater.* **2015**, *5*, 1501355.
[22] X. Liang, A. Garsuch, L. F. Nazar, *Angew. Chem. Int. Ed.* **2015**, *54*, 3907.
[23] a) Q. Pang, D. Kundu, M. Cuisinier, L. F. Nazar, *Nat. Commun.* **2014**, *5*, 4759; b) X. Y. Tao, J. G. Wang, Z. G. Ying, Q. X. Cai, G. Y. Zheng, Y. P. Gan, H. Huang, Y. Xia, C. Liang, W. K. Zhang, Y. Cui, *Nano Lett.* **2014**, *14*, 5288; c) Y. Zhou, C. G. Zhou, Q. Y. Li, C. J. Yan, B. Han, K. S. Xia, Q. Gao, J. P. Wu, *Adv. Mater.* **2015**, *27*, 3774; d) Z. B. Xiao, Z. Yang, L. Wang, H. G. Nie, M. E. Zhong, Q. Q. Lai, X. J. Xu, L. J. Zhang, S. M. Huang, *Adv. Mater.* **2015**, *27*, 2891.
[24] a) H. B. Yao, K. Yan, W. Y. Li, G. Y. Zheng, D. S. Kong, Z. W. Seh, V. K. Narasimhan, Z. Liang, Y. Cui, *Energy Environ. Sci.* **2014**, *7*, 3381; b) Z. W. Seh, J. H. Yu, W. Li, P. C. Hsu, H. Wang, Y. Sun, H. Yao, Q. Zhang, Y. Cui, *Nat. Commun.* **2014**, *5*, 5017.
[25] G. Zhou, L.-C. Yin, D.-W. Wang, L. Li, S. Pei, I. R. Gentle, F. Li, H.-M. Cheng, *ACS Nano* **2013**, *7*, 5367.
[26] H. B. Yao, G. Y. Zheng, P. C. Hsu, D. S. Kong, J. J. Cha, W. Y. Li, Z. W. Seh, M. T. McDowell, K. Yan, Z. Liang, V. K. Narasimhan, Y. Cui, *Nat. Commun.* **2014**, *5*, 3943.
[27] a) Z. Ji, B. Han, Q. Y. Li, C. G. Zhou, Q. Gao, K. S. Xia, J. P. Wu, *J. Phys. Chem. C* **2015**, *119*, 20495; b) Z. G. Wang, X. Y. Niu, J. Xiao, C. M. Wang, J. Liu, F. Gao, *RSC Adv.* **2013**, *3*, 16775; c) T. Z. Hou, H. J. Peng, J. Q. Huang, Q. Zhang, B. Li, *2D Mater.* **2015**, *2*, 014011.
[28] Q. F. Zhang, Y. P. Wang, Z. W. Seh, Z. H. Fu, R. F. Zhang, Y. Cui, *Nano Lett.* **2015**, *15*, 3780.
[29] a) M.-Q. Zhao, H.-J. Peng, G.-L. Tian, Q. Zhang, J.-Q. Huang, X.-B. Cheng, C. Tang, F. Wei, *Adv. Mater.* **2014**, *26*, 7051; b) J. Song, Z. Yu, M. L. Gordin, D. Wang, *Nano Lett.* **2016**, *16*, 864; c) Y.-L. Ding, P. Kopold, K. Hahn, P. A. van Aken, J. Maier, Y. Yu, *Adv. Funct. Mater.* **2016**, *26*, 1112.
[30] a) S. S. Yu, W. T. Zheng, Q. B. Wen, Q. Jiang, *Carbon* **2008**, *46*, 537; b) Z. H. Zhao, M. T. Li, L. P. Zhang, L. M. Dai, Z. H. Xia, *Adv. Mater.* **2015**, *27*, 6834.
[31] a) Y. Jiao, Y. Zheng, M. Jaroniec, S. Z. Qiao, *J. Am. Chem. Soc.* **2014**, *136*, 4394; b) A. Liu, W. Li, H. Jin, X. Yu, Y. Bu, Y. He, H. Huang, S. Wang, J. Wang, *Electrochim. Acta* **2015**, *177*, 36.
[32] Z. Yang, Z. Yao, G. Li, G. Fang, H. Nie, Z. Liu, X. Zhou, X. Chen, S. Huang, *ACS Nano* **2012**, *6*, 205.
[33] M. Wild, L. O'Neill, T. Zhang, R. Purkayastha, G. Minton, M. Marinescu, G. J. Offer, *Energy Environ. Sci.* **2015**, *8*, 3477.
[34] A. B. Sannigrahi, T. Kar, B. G. Niyogi, P. Hobza, P. V. R. Schleyer, *Chem. Rev.* **1990**, *90*, 1061.
[35] H. J. Peng, T. Z. Hou, Q. Zhang, J. Q. Huang, X. B. Cheng, M. Q. Guo, Z. Yuan, L. Y. He, F. Wei, *Adv. Mater. Interfaces* **2014**, *1*, 1400227.
[36] a) B. Delley, *Mol. Simul.* **2006**, *32*, 117; b) A. Klamt, G. Schüürmann, *J. Chem. Soc. Perkin Trans.* **1993**, 799.
[37] K. Xu, *Chem. Rev.* **2004**, *104*, 4303.
[38] a) B. Delley, *J. Chem. Phys.* **1990**, *92*, 508; b) B. Delley, *J. Chem. Phys.* **2000**, *113*, 7756.
[39] J. P. Perdew, K. Burke, M. Ernzerhof, *Phys. Rev. Lett.* **1996**, *77*, 3865.

Received: March 9, 2016
Published online: May 11, 2016

